A Space-Time Multigrid Method for the Numerical Valuation of Barrier Options

John C. Urschel[1]

Abstract

We introduce an adaptive space-time multigrid method for the pricing of barrier options. In particular, we consider the numerical valuation of up-and-out options by the method of lines. We treat both the implicit Euler and Crank-Nicolson methods. We implement a space-time multigrid method in which the domain in space and time are treated simultaneously. We consider an adaptive coarsening technique in which the choice of restriction operator is dependent on the grid's degree of anisotropy at each level. We perform local Fourier analysis to find a suitable choice of our anisotropy constant. We detail the advantages and disadvantages of our technique. In particular, we stress that our algorithm is extremely well suited for parallel computing and, with a suitable smoother, has parallel complexity $O(\log M + \log N)$, allowing for fast computation of extremely large scale problems.

[1] Department of Mathematics, Penn State University.

1   Introduction

The numerical computation of the fair value price of a given barrier option is a particularly relevant problem in finance, due to the lack of closed-form representations for their valuation under the majority of models. There exist nuances for the case of the barrier option that separates it from the general vanilla case. Options with a barrier are extremely sensitive to mispecifications in parameter estimation, due to the discontinuitites in the payoffs, leading to large Gamma ($\Gamma = \frac{\partial^2 V}{\partial S^2}$) and Vega ($\nu = \frac{\partial V}{\partial \sigma}$), and resulting in large pricing errors [1]. We have closed form solutions for the Black Scholes model, however, in cases where more sophisticated volatility models are used, exact solutions no longer exist. However, due to reasons stated above, such volatility models are particularly useful for barrier options.

There exists a number of different techniques for pricing options. In particular, the two main techniques used in practice are to estimate the price by Monte Carlo methods or by solving the corresponding partial differential equation (PDE). We consider the latter approach exclusively. The PDE approach requires the computation of the solution of a second order linear parabolic equation. We consider discretization by the method of lines with finite differences. We apply multigrid (MG) methods to the given discretization, treating the entire grid simultaneously and introducing an adaptive restriction procedure that depends on the PDE's characteristics and the given discretization.

Treating the entire grid simultaneously allows for full parallelization of the algorithm. For a grid with N points in space and M in time, multigrid in space with time-stepping has parallel complexity $O(M \log N)$. In contrast, treating the grid as a whole with a suitable smoother results in parallel complexity $O(\log M + \log N)$. For fine grids, this difference is significant; even for extremely large probems the parallel complexity of our algorithm is nominal.

The flow of the paper is as follows. We begin by introducing the mathematical framework of our problem. We give the numerical details of our method for the Black-Scholes operator by finite differences. We then detail the technique used to determine the restriction operator and give numerical results. We show our method to be robust to more general volatility models and consider the CEV model as an example. In addition, we give a discussion of our method in general, considering both its advantages and disadvantages.

Figure 1: Plot of a stock that crosses the barrier

Figure 2: Plot of a stock that doesn't cross the barrier

2   Mathematical Framework

A barrier option is a given derivative with an additional condition on its movement. In particular, a stock level B is set and the stock's movement is observed over the life of the option $[0, T]$. Depending on the type of barrier, the option will become worthless if the extra condition involving the stock price level B is not satisfied. Thus a barrier option will have the payoff of a call or a put, unless it is rendered worthless by an additional condition. There are predominantly eight different types of barrier options, depending on the choice of call or put, up or down, and in or out. We assume our options to be European in nature and contain a single continuous barrier. We have the following formal definition.

Definition 2.1. *A barrier option is a call or put derivative with an additional condition for the path of the underlying S_t with respect to a given level of stock price B. An up-and-out barrier option is worthless if there exists a $t \in [0, T)$ such that $S_t \geq B$. An up-and-in barrier option is worthless if there does not exist a $t \in [0, T)$ such that $S_t \geq B$. A down-and-out barrier option is worthless if there exists a $t \in [0, T)$ such that $S_t \leq B$. A down-and-in barrier option is worthless if there does not exist a $t \in [0, T)$ such that $S_t \leq B$.*

In this paper, we consider the up-and-out European call option. In Figures 1 and 2, we see two realizations of the underlying stock. In Figure 1, we see that the stock crosses the boundary and the option expires worthless. However, in Figure 2 the stock does not cross the boundary, and therefore the option expires as a standard call, with value $|S_T - K|_+$. We give a list of the types of barrier options in Table 1, along with their worth, based on interaction with

Table 1: Types of Single Barrier Options

Option	Type	Barrier	Crossed	Not Crossed
Call	Down-and-Out	Below Spot	Worthless	Standard Call
	Down-and-In	Below Spot	Standard Call	Worthless
	Up-and-Out	Above Spot	Worthless	Standard Call
	Up-and-In	Above Spot	Standard Call	Worthless
Put	Down-and-Out	Below Spot	Worthless	Standard Call
	Down-and-In	Below Spot	Standard Call	Worthless
	Up-and-Out	Above Spot	Worthless	Standard Call
	Up-and-In	Above Spot	Standard Call	Worthless

the barrier. We note that, of these eight types, there are only four independent cases. The sum of an up-and-in (or down-and-in) and an up-and-out (or down-and-out) gives a vanilla option.

We take our underlying to be given by

$$dS(t) = \beta(S(t))\, dt + \gamma(S(t))\, d\tilde{W}(t) \tag{1}$$

where $\tilde{W}(t)$, $0 \le t \le T$, is a Brownian motion on the risk neutral measure $\tilde{\mathbb{P}}$. By the Feymann-Kac formula[2], the fair price of an up-and-out call option at time t, $v(x,t) = \mathbb{E}^{x,t}[e^{-r(T-t)}v(x,T)]$, is the solution to the PDE

$$\frac{\partial v}{\partial t} + \beta(x,t)\,\frac{\partial v}{\partial x} + \frac{1}{2}\,\gamma(x,t)^2\,\frac{\partial^2 v}{\partial x^2} - rv = 0 \tag{2}$$

with terminal condition $v(x,T) = |x - K|_+$ and boundary conditions $v(0,t) = v(B,t) = 0$. Depending on the model, the choice of β and γ varies. However, for now we assume $\beta(x,t) = rx$ and $\gamma(x,t) = \sigma x$, r, σ constant. This gives us the Black-Scholes PDE. We save treatment of more general choices of γ to Section 5.

---

[2]The author notes that a significant amount of subtlety regarding the applicability of the Markov property and the Feymann-Kac Theorem has been neglected. For a more detailed analysis of why the PDE for the barrier option is the same as for the vanilla option and the process to come to this result, refer to [2].

Through a coordinate transformation of the Black-Scholes PDE, one can obtain the heat equation [3]. We consider the transformation $x = e^y$, $t = T - \frac{2\tau}{\sigma^2}$. This gives us the PDE $v_\tau = v_{yy} + (\frac{2r}{\sigma^2} - 1)v_y - \frac{2r}{\sigma^2}v$. Setting $v(y,\tau) = e^{\alpha y + \beta \tau} u(y,\tau)$, with $\alpha = \frac{\sigma^2 - 2r}{2\sigma^2}$ and $\beta = (\frac{\sigma^2 + 2r}{2\sigma^2})^2$, we obtain the heat equation on the transformed domain $(y,\tau) \in (-\infty, \ln B) \times (0, \frac{\sigma^2}{2}T]$, with initial condition $u(y,0) = e^{-\alpha y}|e^y - K|_+$ and boundary condition $\lim_{y \to -\infty} u(y,\tau) = u(\ln B, \tau) = 0$. For any solution obtained by the heat equation in the transformed domain, the corresponding fair option value can be obtained by multiplying by $e^{\alpha y + \beta \tau}$ and transforming $(y,\tau) \to (x,t)$. This transformed domain is preferred for local Fourier analysis and, therefore, significantly more suitable for our method.

3   Numerical Formulation

We consider the discretizion of our transformed PDE. Because of the infinite lower boundary in space, we must set an artificial lower boundary. We choose $-\ln B$, which transforms to a value of $\frac{1}{B}$ in the standard domain and, for reasonably large B, is sufficiently close to zero[3]. We define a partition in space $\Pi_x = \{x_1, x_2, ..., x_{N-1}, x_N\}$, where $-\ln B = x_1 < x_2 < ... < x_{N-1} < x_N = \ln B$, $h_x = x_{j+1} - x_j$. We implement a centered difference quotient in space to approximate our problem by a system of $N - 2$ ODE's. Some of the common first- and second-order numerical techniques for solving ODE initial value problems include the implicit and explicit Euler methods, the midpoint method, and the trapezoidal rule. Both the explicit Euler and midpoint method are explicit in nature and exhibit limited stability domains. We will restrict ourselves to the implicit Euler method and the Crank-Nicolson method[4].

Both the implict Euler and Crank-Nicolson methods have their advantages. The Crank-Nicolson method is of higher order and more commonly used in practice. However, it can result in oscillatory behavior in the solutions, due to

---

[3]The error of this approximation can be explicitly calculated by computing the difference in solution between an up-and-out and double knock-out call with lower barrier at $\frac{1}{B}$

[4]When applied to a PDE via the method of lines, the trapezoidal rule is commonly referred to as the Crank-Nicolson method

the non-smooth (and possiblity jump) initial conditions that occur in option pricing [4]. There are a number of ways to avoid this issue, and reasonable augmentations of the method can be found in [5]. To apply these methods, we introduce a partition in time $\Pi_t = \{t_1, t_2, ..., t_{M-1}, t_M\}$, with $0 = t_1 < t_2 < ... < t_{M-1} < t_M = T$, $h_t = t_i - t_{i-1}$. We have the stencils

$$
\begin{bmatrix}
0 & 0 & 0 \\
-\frac{h_t}{h_x^2} & 1 + \frac{2h_t}{h_x^2} & -\frac{h_t}{h_x^2} \\
0 & -1 & 0
\end{bmatrix}, \qquad
\begin{bmatrix}
0 & 0 & 0 \\
-\frac{h_t}{2h_x^2} & 1 + \frac{h_t}{h_x^2} & -\frac{h_t}{2h_x^2} \\
-\frac{h_t}{2h_x^2} & -1 + \frac{h_t}{h_x^2} & -\frac{h_t}{2h_x^2}
\end{bmatrix}
\tag{3}
$$

for the implicit Euler and Crank-Nicolson methods, respectively. This gives a system of $(M - 1) \times (N - 2)$ equations. We consider solving the discretized system by multigrid methods.

Multigrid (MG) methods are a class of techniques used to solve discrete formulations of differential equations by utilizing a multilevel grid structure. Most pointwise relaxation schemes (such as Gauss-Seidel, Jacobi, etc.) have different rates of convergence for the low and high frequency components of the error. In particular, the high frequency components are tough to smooth. Due to the aliasing effect of restriction operators on the frequency domain of the error, coarse grids can be used to effectively smooth the high frequency components. Interpolation between grids is used to create a multilevel structure to maintain the smoothing effects of the pointwise smoother on the low frequency components, while also smoothing the high frequency components through the coarse grids [6].

There are a number of ways to perform an effective multilevel scheme. We consider the multigrid V-cycle. This choice is mainly for simplicity, and a W-cycle or full multigrid (FMG) cycle could also suffice, although V-cycles have been shown to be better suited to parallelization. We detail the generic MG-cycle in Algorithm 3. Taking $\gamma = 1$ gives us the V-cycle.

We consider Gauss-Seidel red-black smoothing. Another technique (such as Jacobi, Richardson, etc.) can be used, but, in general, Gauss-Seidel has been shown to be the most effective pointwise smoother for multigrid techniques [3]. We choose red-black ordering rather than lexicographic because of the ease with which it can be parallelized.

[H] Multigrid Cycle $u_k^{m+1} = MGCYCLE(k, \gamma, A_k, u_k^m, f_k, \nu_1, \nu_2)$

Pre-Smoothing:

$\tilde{u}_k^m = S^{\nu_1} u_k^m$

Coarse-Grid Correction:

$r_k = f_k - A_k \tilde{u}_k^m$

$r_{k-1} = I_k^{k-1} r_k$

Approximate Coarse Solution:

If $k = 1$

Solve $A_0 e_0 = r_0$ Exactly

$e_0 = A_0^{-1} r_0$

Else

Solve $A_{k-1} e_{k-1} = r_{k-1}$ Approximately with γ MG Cycle Calls

$e_{k-1} = MGCYCLE^{\gamma}(k-1, \gamma, A_{k-1}, 0, r_{k-1}, \nu_1, \nu_2)$

Interpolate Correction:

$e_k = I_{k-1}^k e_{k-1}$

$u_k^{CGC} = \tilde{u}_k^m + e_k$

Post-Smoothing:

$u_k^{m+1} = S^{\nu_2} u_k^{CGC}$

For interpolation, we implement a restriction operator whose properties depend on the given grid level. In particular, we consider the anisotropy ratio $\frac{h_t}{h_x^2}$. We determine the value of $\frac{h_t}{h_x^2}$ for which coarsening in time and in space produce equivalent two-grid convergence rates (denoted λ_a), and use it as a cutoff for our choice of coarsening in space or time. We stress that simulatneous coarsening cannot be used effectively; the anisotropy ratio approaches zero fairly quickly on coarser grids, resulting in a divergent smoother. The stencils for the space, time, and simultaneous restriction operators, respectively, are given below.

$$\frac{1}{4}\begin{bmatrix} 0 & 0 & 0 \\ 1 & 2 & 1 \\ 0 & 0 & 0 \end{bmatrix} \qquad \frac{1}{2}\begin{bmatrix} 0 & 0 & 0 \\ 0 & 1 & 0 \\ 0 & 1 & 0 \end{bmatrix} \qquad \frac{1}{8}\begin{bmatrix} 0 & 0 & 0 \\ 1 & 2 & 1 \\ 1 & 2 & 1 \end{bmatrix} \qquad (4)$$

The time restriction operator is asymmetric, so as to not transfer any information backward in time. The prolongation operators are taken to be the adjoints of the restriction operators. The process used to determine the value

of λ_a explicitly is the subject of Section 4.

4   Local Mode Analysis

We consider the application of local mode analysis to our discretized problem. We aim to produce an anisotropy ratio $\lambda_a := \frac{h_t}{h_x^2}$ to determine whether coarsening in space or time produces a preferable convergence rate on a given grid level. The work in this section follows from [6, 7].

We are unable to perform rigorous Fourier analysis for the majority of cases because it requires the existence of an orthogonal basis of periodic eigenfunctions for the operator. Rigorous Fourier analysis can only be applied to a very small class of problems in practice [8]. It is for this reason we turn to local Fourier analysis. This technique was first introduced by Brandt [9]. The analysis is performed locally, and assumes our problem to be a linear differential equation with constant coefficients. In general, the equations dealt with in option pricing do not fit this criteria, but locally can be assumed to be of this form. However, problems can occur when attempting to produce a result for an entire grid. In this case, a suitable freezing of coefficients must be chosen. In Section 4.2 we discuss the forms of non-constant coefficient parabolic PDEs that are well suited to this analysis and, more importantly, our technique.

We begin by detailing the local Fourier analysis technique in two dimensions. We aim to approximate the spectral matrix of the two-grid operator

$$M_h^H = S_h^{\nu_2}(I_h - I_H^h L_H^{-1} I_h^H F_h L_h)S_h^{\nu_1},$$

where S_h is a given smoothing operator, ν_1 and ν_2 are the number of pre- and post-smoothing iterations performed, I_h is the identity operator, and I_h^H and I_H^h are the restriction and prolongation operators, respectively. We use F_h as a normalizing constant; we have $F_h = 1$ for space coarsening and $F_h = 2$ for time and simultaneous coarsening. We attempt to approximate M_h^H using an operator $\hat{M}_h^H$ defined on the frequency domain of our problem. We define the frequency domain operator $\hat{M}_h^H$ in similar way:

$$\hat{M}_h^H = \hat{S}_h^{\nu_2}(\hat{I}_h - \hat{I}_H^h \hat{L}_H^{-1} \hat{I}_h^H F_h \hat{L}_h)\hat{S}_h^{\nu_1}.$$

Each operator is represented by a 4×4 matrix acting on the frequency domain
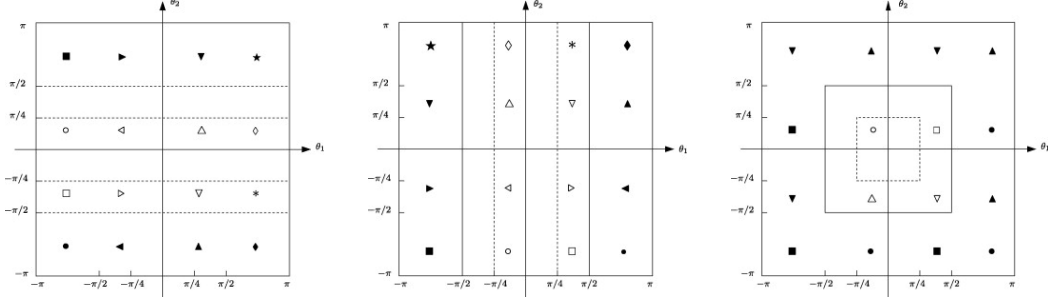
Figure 3: Aliasing Fourier modes for coarsening in space, in time, and in space and time, respectively. White shapes represent coarse grid modes, black shapes represent fine grid modes. The coarse grid modes that each fine grid aliases with is denoted by the same shape.

$[-\pi, \pi)^2$. For our purposes we have $(I_h^H)^T = I_H^h$ and $(\hat{I}_h^H)^T = \hat{I}_H^h$, but this is not always the case.

We define $\Theta_h = \{(\theta_1, \theta_2) : \theta_\alpha = 2\pi k_\alpha / n_\alpha\}$, $k_\alpha = -n_\alpha/2 + 1, ..., n_\alpha/2$ ($k_1 = M$, $k_2 = N$) to be a discretization of the frequency domain. Given some $\theta^1 \in \Theta_h \cap [-\pi/2, \pi/2)^2$, we define the following vectors.

$$\theta^2 = \theta^1 - \begin{pmatrix} sign(\theta_1^1)\pi \\ sign(\theta_2^1)\pi \end{pmatrix} \qquad \theta^3 = \theta^1 - \begin{pmatrix} 0 \\ sign(\theta_2^1)\pi \end{pmatrix} \qquad \theta^4 = \theta^1 - \begin{pmatrix} sign(\theta_1^1)\pi \\ 0 \end{pmatrix}$$

We introduce exponential Fourier modes $\psi_h(\theta)_j = e^{ij\cdot\theta}$, $j = (j_1, j_2)$, $j_\alpha = 0, ..., n_\alpha-1$. For $\theta \in \Theta_h \cap [-\pi/2, \pi/2)^2$, we define $\Psi_h(\theta) = (\psi_h(\theta^1), \psi_h(\theta^2), \psi_h(\theta^3), \psi_h(\theta^4))^T$. We note that the linear space spanned by $\Psi_h(\theta)$ is invariant under the two-grid operator $\hat{M}_h^H(\theta)$. We see that when $\psi_h(\theta)$ is projected to the coarse grid, it aliases with $\psi_H(\bar{\theta})$, where $\bar{\theta}$ equals $(2\theta_1, \theta_2)$ for coarsening in space, $(\theta_1, 2\theta_2)$ for coarsening in time, and $(2\theta_1, 2\theta_2)$ for simultaneous coarsening. We give Figure 3, from [10], to illustrate this for the three different cases.

All that remains is to consider the representations for $\hat{L}_h$, $\hat{L}_H$, $\hat{I}_h^H$, and $\hat{S}_h$. Let l_k, s_k, r_k, and p_k represent the stencils for L_h, L_H, I_H^h and I_h^H, respectively, where k ranges over an index set $J \subset \mathbb{Z}^2$. We begin with $\hat{L}_h$; its representation is given by

$$\hat{L}_h(\theta) = \begin{pmatrix} \tilde{L}_h(\theta^1) & 0 & 0 & 0 \\ 0 & \tilde{L}_h(\theta^2) & 0 & 0 \\ 0 & 0 & \tilde{L}_h(\theta^3) & 0 \\ 0 & 0 & 0 & \tilde{L}_h(\theta^4) \end{pmatrix},$$

where $\tilde{L}_h(\theta) = \sum_{k\in J} l_k e^{ik\cdot\theta}$. For the coarse grid $\hat{L}_H$, we have

$$\hat{L}_H(\theta) = \begin{pmatrix} \tilde{L}_H(\bar{\theta}^1) & 0 \\ 0 & \tilde{L}_H(\bar{\theta}^3) \end{pmatrix}, \begin{pmatrix} \tilde{L}_H(\bar{\theta}^1) & 0 \\ 0 & \tilde{L}_H(\bar{\theta}^4) \end{pmatrix}, \qquad \left(\tilde{L}_H(\bar{\theta}^1) \right)$$

for coarsening in space, time, and space and time, respectively. Similarly to $\tilde{L}_h(\theta)$, we have $\tilde{L}_H(\theta) = \sum_{k\in J} s_k e^{ik\cdot\theta}$. The prologation operator $\hat{I}_H^h(\theta)$ is represented by

$$\hat{I}_H^h(\theta) = \begin{pmatrix} \tilde{I}_H^h(\theta^1) & 0 \\ 0 & \tilde{I}_H^h(\theta^2) \\ 0 & \tilde{I}_H^h(\theta^3) \\ \tilde{I}_H^h(\theta^4) & 0 \end{pmatrix}, \begin{pmatrix} \tilde{I}_H^h(\theta^1) & 0 \\ 0 & \tilde{I}_H^h(\theta^2) \\ \tilde{I}_H^h(\theta^3) & 0 \\ 0 & \tilde{I}_H^h(\theta^4) \end{pmatrix}, \begin{pmatrix} \tilde{I}_H^h(\theta^1) \\ \tilde{I}_H^h(\theta^2) \\ \tilde{I}_H^h(\theta^3) \\ \tilde{I}_H^h(\theta^4) \end{pmatrix}$$

for coarsening in space, time, and space and time, respectively. We have $\tilde{I}_H^h$ given by $\tilde{I}_H^h(\theta) = \frac{h_1 h_2}{H_1 H_2} \sum_{k\in J} p_{-k} e^{ik\cdot\theta}$. The operator $\hat{S}_h(\theta)$ for Gauss-Seidel red-black smoothing has the form

$$\hat{S}_h(\theta) = \frac{1}{2} \begin{pmatrix} \alpha(\theta^1) + \beta(\theta^1) & \alpha(\theta^2) - \beta(\theta^2) & 0 & 0 \\ \alpha(\theta^1) - \beta(\theta^1) & \alpha(\theta^2) + \beta(\theta^2) & 0 & 0 \\ 0 & 0 & \alpha(\theta^3) + \beta(\theta^3) & \alpha(\theta^4) - \beta(\theta^4) \\ 0 & 0 & \alpha(\theta^3) - \beta(\theta^3) & \alpha(\theta^4) + \beta(\theta^4) \end{pmatrix},$$

where the functions $\alpha(\theta)$ and $\beta(\theta)$ have the representations

$$\alpha(\theta) = -\frac{1}{l_{(0,0)}} \sum_{k\in J_0} l_k e^{ik\cdot\theta}, \qquad \beta(\theta) = -\frac{1}{l_{(0,0)}} \left(\sum_{|k|=odd} l_k \alpha(\theta) e^{ik\cdot\theta} + \sum_{0\neq|k|=even} l_k e^{ik\cdot\theta} \right),$$

with $J_0 = J\backslash\{(0,0)\}$ and $|k| = |k_1| + |k_2|$. The interpolation elements are independent of the specific parabolic PDE and choice of numerical ODE method. We give the following representations for the prolongation elements.

$$_s\tilde{I}_H^h(\theta) = \frac{1 + \cos(\theta_1)}{2} \qquad _t\tilde{I}_H^h(\theta) = \frac{1 + e^{-i\theta_2}}{2} \qquad _{st}\tilde{I}_H^h(\theta) = \, _s\tilde{I}_H^h(\theta) \, _t\tilde{I}_H^h(\theta)$$

What remains to be considered are the representations for the elements of the PDE itself and the smoother, which vary by equation and discretization. We

include the elements for the transformed Black-Scholes PDE.

$$_{ie}\tilde{L}_h(\theta) = 1 - e^{-i\theta_2} + 2\lambda(1 - \cos(\theta_1))$$

$$_{ie}\alpha(\theta) = \frac{e^{-i\theta_2} + 2\lambda\cos(\theta_1)}{1 + 2\lambda}$$

$$_{ie}\beta(\theta) = \alpha^2(\theta)$$

$$_{cn}\tilde{L}_h(\theta) = 1 - e^{-i\theta_2} + \lambda(1 - \cos(\theta_1))(1 + e^{-i\theta_2})$$

$$_{cn}\alpha(\theta) = \frac{(1 - \lambda)e^{-i\theta_2} + \lambda\cos(\theta_1)(1 + e^{-i\theta_2})}{1 + \lambda}$$

$$_{cn}\beta(\theta) = \frac{(1 - \lambda)\alpha(\theta)e^{-i\theta_2} + \lambda\cos(\theta_1)(\alpha(\theta) + e^{-i\theta_2})}{1 + \lambda}$$

4.1   Numerical Results

We consider the numerical application of our multigrid method, using local Fourier analysis to determine our restriction operator. Using the explicit representations of the stencils of the operators in the frequency domain, we can compute the spectral radius of $\hat{M}_h^H$ for a given $\theta \in \Theta_h \cap [-\pi/2, \pi/2)^2$. We define $\tilde{\rho} = \max\{\rho(\hat{M}_h^H) \mid \theta \in \Theta_h \cap [-\pi/2, \pi/2)^2\}$, where $\rho(\cdot)$ is the spectral radius. This gives an indicative measure of the convergence rate for a given choice of λ_a and restriction operator. We note that the computational cost of determining λ_a is nominal in comparison to a multigrid iteration.

For numerical illustration, we consider the problem of pricing an up-and-out call barrier option with the following conditions:

$$B = 20, \ K = 13, \ T = 1, \ r = 0.1, \ \sigma = 0.25. \tag{5}$$

For the test problem (5), we computed $\tilde{\rho}$ for a range of values of λ. We consider the value of λ for which $\tilde{\rho}_x \approx \tilde{\rho}_t$. For the implicit Euler method this value is clear and well-defined, but for the Crank-Nicolson method, which exhibits more erratic behavior with respect to λ, there are a number of such values. For this case, the choice of λ_a is somewhat qualitative. We take $\lambda_a = 2^{-3/4}$ for the implicit Euler method and $\lambda_a = 2^{-1}$ for the Crank-Nicolson method.

Table 2: Convergence Factors for Adaptive Space-Time V-Cycle(2,2)

Method	M \ N	Standard Domain			Transformed Domain		
		33	65	129	33	65	129
	33	.1391	.4103	.6738	.0010	.0057	.1016
Implicit Euler	65	.1597	.4078	.6715	.0218	.0589	.1395
	129	.2833	.5532	.7142	.1868	.2288	.2604
	33	.0097	.0967	.2673	.0004	.0025	.0143
Crank-Nicolson	65	.0583	.0922	.2407	.0201	.0414	.0643
	129	.1890	.2264	.3200	.1914	.1473	.1763

We consider convergence results for the given test problem. We compute numerical tests for both the standard and transformed Black-Scholes PDE. For the standard domain, we freeze x at $B/\sqrt{2}$. To determine λ_a for the standard domain, it suffices to divide the value of λ_a for the transformed domain by $\frac{\sigma^2 B^2}{4} = \frac{25}{4} \approx 2^{11/4}$. This can be justified by considering $u_t = \frac{1}{2}\sigma^2 x^2 u_{xx}$ and noting the nominal effect lower order terms play in local Fourier analysis.

We compute approximate convergence rates for different grid sizes, using $\left(\frac{d^{(n)}}{d^{(j)}}\right)^{(1/(n-j))}$ as a measure of convergence, where $d^{(i)} = f - Au^{(i)}$ and n is the number of iterations for $d^{(i)}$ to satisfy the given tolerance $||d^{(i)}|| < c$. For our tests, we take $c = MN \times 10^{-15}$. Often in Multigrid tests, j is chosen to be a small, nonzero number such that the true convergence can be seen. We take $j = 3$. We have the results in Table 2.

We see immediately that the convergence rates in the transformed domain are superior to that of the standard domain. We see that the extra assumption of a constant coefficient operator, especially in the terms of higher differential order, is one that greatly affects the results. We stress this trend for our method, and will give more rigorous justification in Section 4.2.

4.2 Local Fourier Analysis for Parabolic Equations in $\mathbb{R}^d$

It can be seen that the process of local Fourier analysis does not apply well to PDEs with non-constant coefficients in the higher differential order terms. Although a constant coefficient PDE is ideal, the form $u_t = \Delta u + \delta(x)u$ is the next best choice. Under suitable conditions, we can put strict bounds on the pertubations of the two-grid analysis. We stress the importance of two-grid convergence results that are robust to the entire domain. Before giving such results, we must give the formulation of local mode analysis for parabolic equations in $\mathbb{R}^d$.

We consider the frequency domain $[-\pi, \pi)^{d+1}$, coupled with some discretization $\Theta_h = \{\theta : \theta_\alpha = 2\pi k_\alpha / n_\alpha, k_\alpha = -n_\alpha/2 + 1, ..., n_\alpha/2\}$. We assume θ_{d+1} to be the frequency component of the time variable. Given a choice $\theta \in \Theta_h \cap [-\pi/2, \pi/2)^{d+1}$, we can define 2^{d+1} vectors $\theta^1, \theta^2, ..., \theta^{2^{d+1}}$ by

$$\theta^m = \theta - \Gamma,$$

where $\Gamma_i := \mathbf{1}_{i \in \mathcal{C}_m} sgn(\theta_i)\pi$, and $\{\mathcal{C}_i\}_1^{2^{d+1}}$ are the 2^{d+1} different combinations of the set $\mathbb{Z}_{d+1} = \{1, ..., d+1\}$. Therefore, each operator in the frequency domain is represented by a $2^{d+1} \times 2^{d+1}$ matrix. The exponential Fourier mode $\phi_h(\theta)$ aliases with $\phi_H(\bar{\theta})$ upon restriction, with $\bar{\theta}$ equal to $(2\theta_1, 2\theta_2, ..., 2\theta_d, \theta_{d+1})$ for coarsening in space, $(\theta_1, \theta_2, ..., \theta_d, 2\theta_{d+1})$ for coarsening in time, and $(2\theta_1, 2\theta_2, ..., 2\theta_d, 2\theta_{d+1})$ for simultaneous coarsening. The extensions of the operators from the case of $\mathbb{R}^2$ to $\mathbb{R}^{d+1}$ are natural and omitted. However, we note that the interpolation operators are dependent on the ordering of the combinations $\{\mathcal{C}_i\}_{i=1}^{2^{d+1}}$. We present the following result.

Theorem 4.1. *Let $\hat{M}_h^H$ and $(\hat{M}_h^H)^{\Delta+\delta}$ be the two-grid frequency domain operators of the method of lines discretization (using implicit Euler or Crank-Nicolson) of $u_t = \Delta u$ and $u_t = \Delta u + \delta(x)u$, respectively. Let $\hat{E}_{2G} = \hat{I}_h - \hat{I}_H^h \hat{L}_H^{-1} \hat{I}_h^H F_h \hat{L}_h$, $\Lambda = \sum_{i=1}^d \frac{h_t}{h_{x_i}^2}$, $\epsilon = \min_{\theta \in \Theta_h} \tilde{L}_h(\theta)$, and $\Xi = \max_{\theta \in \Theta_h} \|\hat{E}_{2G}\|$. Suppose that Θ_h is bounded away from a neighborhood of zero. In addition, suppose that h_t is sufficiently small, and that a smoothing property holds, namely, $h_t \delta(x) < \min(\frac{\epsilon}{2}, \Lambda)$ and $\alpha(\theta) < 1$. Then we have*

$$\max_{\theta \in \Theta_h} |\rho[\hat{M}_h^H(\theta)] - \rho[(\hat{M}_h^H)^{\Delta+\delta}(\theta; x)]| \leq C h_t \delta(x), \tag{6}$$

with $C = \frac{4(\nu_1+\nu_2)}{1+\Lambda/2}\Xi + \frac{1+5(1+\Xi)}{F_h\epsilon} + O(h_t\delta(x))$.

The above theorem is quite technical in nature, but the intuition gained is that the variation in the results of local mode analysis is small for h_t sufficiently small. Therefore, for a reasonably fine grid, the results of local mode analysis for a given freezing of coefficients is fairly robust. The proof is left to the appendix.

We note that the terms ϵ and Ξ are $O(1)$ and are of reasonable value when the grid in the frequency domain is sufficiently far away from zero. Our operator $\hat{L}_h$ is degenerate at zero, but for a rough mesh that avoids zero in the frequency domain, ϵ is large enough. Assuming $n = n_\alpha$ for all α, n odd, one can compute the bound $\epsilon \geq \frac{\pi^2}{n^2}(1 - \frac{\pi^2}{n^2})\Lambda$ by Taylor expansion of the cosine function.

For a PDE that cannot be converted to a constant coefficient differential equation, we will settle for the form $u_t = \Delta u + \delta(x)u$. A small amount of variance in our two-grid convergence results is acceptable and affects the cutoff nominally. Theorem 4.1 allows us to apply our method to a larger class of models and be assured that our method will perform well.

5 Deterministic Volatility Models

In practice, the Black-Scholes model is far from practical, and does not give a true representation of the behavior of the volatility. The model fails to capture the volatility "smile". A common technique to overcome the model's shortcomings is to use deterministic volatility models. The deterministic volatility approach models the volatility as a deterministic function of the underlying. The volatility function is calibrated so that it accurately captures the volatility smile. These models are sometimes referred to as one-factor models, stemming from the single source of randomness. Advantages of such an approach is that it produces functions that are monotonic with respect to the underlying (for vanilla options), perfectly correlated with the underlying, and replicable [11]. The main example of such an approach is the constant elasticity of variance (CEV) model.

For general deterministic volatility models we assume our underlying to be

given by the stochastic differential equation

$$dS(t) = rS(t)\,dt + \gamma(S(t))\,d\tilde{W}(t),\tag{7}$$

resulting in the PDE

$$\frac{\partial v}{\partial t} + rx\,\frac{\partial v}{\partial x} + \frac{1}{2}\,\gamma(x)^2\,\frac{\partial^2 v}{\partial x^2} - rv = 0.\tag{8}$$

Through the transformation[5] $y = \phi(x) := \int \sqrt{2}[\gamma(x)]^{-1}dx, \tau = T - t$, we obtain $v_\tau = v_{yy} + (rx\phi' + \frac{\phi''}{2}\gamma^2)v_y - rv$. Letting $v(y,\tau) = e^{\psi(y)}u(y,\tau)$, $\psi(y) := \int rx\phi' + \frac{\phi''}{2}\gamma^2 dy$, we have the form $u_\tau = u_{yy} + \delta(y)u$, with $\delta(y) = \psi''(y) - (\psi'(y))^2 - r$.

Our algorithm is nearly identical for this case, with slightly different stencils

$$\begin{bmatrix} 0 & 0 & 0 \\ -\frac{h_t}{h_x^2} & 1 + \frac{2h_t}{h_x^2} - h_t\delta(y) & -\frac{h_t}{h_x^2} \\ 0 & -1 & 0 \end{bmatrix}, \quad \begin{bmatrix} 0 & 0 & 0 \\ -\frac{h_t}{2h_x^2} & 1 + \frac{h_t}{h_x^2} - \frac{h_t}{2}\delta(y) & -\frac{h_t}{2h_x^2} \\ -\frac{h_t}{2h_x^2} & -1 + \frac{h_t}{h_x^2} - \frac{h_t}{2}\delta(y) & -\frac{h_t}{2h_x^2} \end{bmatrix}\tag{9}$$

for the implicit Euler and Crank-Nicolson method, respectively, as well as slightly perturbed LFA elements (refer to the Appendix).

For the special case of the CEV model, we have $\gamma(x) = \sigma x^\beta$, for some $\beta > 0$. This results in

$$\delta_{CEV}(y) = -\left(\frac{\beta}{2(1-\beta)y^2} + \frac{r(1-\beta)}{2}\right) - \left(\frac{\beta}{2(1-\beta)y} - \frac{r(1-\beta)y}{2}\right)^2 - r.\tag{10}$$

6   General Discussion of Technique

Our space-time multigrid technique has both its advantages and disadvantages. We believe the main source of appeal for our algorithm, as well as its drawbacks, to be as follows:

Advantages:

- multigrid techniques are iterative in nature

---

[5]Typically, we have $\gamma(0) = 0$. In this case, we will have $-\infty$ as the lower boundary for our transformed domain, and must create an artificial boundary as we did in Section 3.

- space-time multigrid, with a suitable smoother, is fully parallelizable

- the method is robust to a large class of options and pricing models

Disadvantages:

- treating space and time simultaneously produces large matrices

The advantage of an iterative technique is two-fold. First, the ability to choose a stopping criterion allows the individual to decide whether to favor approximation quality or quicker computations, depending on individual needs. Second, it allows the use of favorable initial approximations, which are readily available for the majority of financial instruments.

In addition, our method is fully parallelizable. In particular, assuming a sufficient amount of processors, our method has parallel complexity $O(\log M + \log N)$ (M and N being the number of grid points in the time and space directions, respectively), as compared to time-stepping methods (such as multigrid in space), which has at best $O(M \log N)$ parallel complexity. Our algorithm comes into its own when the speed of computation is at a premium, rather than overall computational cost.

Through domain transformations, we have shown our method to be robust to a large class of parabolic PDEs. In particular, we have shown our method to be applicable to general deterministic volatility models. Finally, we note that our technique need not be limited to the case of barrier options, and is fully applicable to general derivatives. The choice of options with a barrier was because of the lack of explicit solutions for the majority of models.

The major disadvantage of the method is the large matrix it produces. To gain a great deal of accuracy in the solution, the matrix must become large. However, this matrix is sparse. We stress that this algorithm is not meant to be performed on a single processor. This technique is advantageous when multiple processors are available, and a short computation time is of great importance. The algorithm's ability to be fully parallelized makes the large matrix less relevant, although it does remain a valid point. For a single processor, multigrid in space with time-stepping would be a more suitable procedure.

7 Appendix: Proof of Theorem 4.1

To begin, we consider the difference in stencil elements for $u_t = \Delta u$ and $u_t = \Delta u + \delta(x)u$. We consider the perturbations of each element $\square^{\delta} := \square^{\Delta+\delta} - \square^{\Delta}$. We have the following.

$$_{ie}\tilde{L}_h^{\delta}(\theta) = -h_t\delta(x) \tag{11}$$

$$_{ie}(\tilde{L}_H^{\delta}(\theta))^{-1} = \frac{h_t\delta(x)}{\tilde{L}_H^{\Delta+\delta}(\theta)\tilde{L}_H(\theta)} \tag{12}$$

$$_{ie}\alpha_{\delta}(\theta) = -\frac{h_t\delta(x)\alpha(\theta)}{1 + 2\sum_{i=1}^{d}\lambda_i - h_t\delta(x)} \tag{13}$$

$$_{ie}\beta_{\delta}(\theta) = \big(\alpha_{\delta}(\theta)(1 + e^{-i\theta_{d+1}})\sum_{i=1}^{d}\lambda_i\cos(\theta_i) - h_t\delta\beta(\theta) \tag{14}$$

$$+ \alpha_{\delta}(\theta)e^{-i\theta_{d+1}}(1 - \sum_{i=1}^{d}\lambda_i))/(1 + 2\sum_{i=1}^{d}\lambda_i - h_t\delta(x))$$

$$_{cn}\tilde{L}_h^{\delta}(\theta) = -\frac{1}{2}(1 + e^{-i\theta_{d+1}})h_t\delta(x) \tag{15}$$

$$_{cn}\tilde{L}_H^{-\delta}(\theta) = \frac{\frac{1}{2}(1 + e^{-i\theta_{d+1}})h_t\delta(x)}{\tilde{L}_H^{\Delta+\delta}(\theta)\tilde{L}_H(\theta)} \tag{16}$$

$$_{cn}\alpha_{\delta}(\theta) = -\frac{\frac{h_t}{2}\delta(x)\big(e^{-i\theta_{d+1}} + \alpha(\theta)\big)}{1 + \sum_{i=1}^{d}\lambda_i - \frac{h_t}{2}\delta(x)} \tag{17}$$

$$_{cn}\beta_{\delta}(\theta) = \big(\alpha_{\delta}(\theta)(\alpha(\theta)(1 + \sum_{i=1}^{d}\lambda_i) - e^{-i\theta_{d+1}}\sum_{i=1}^{d}\lambda_i\cos(\theta_i)) \tag{18}$$

$$- \frac{h_t}{2}\delta(x)(\alpha(\theta)e^{-i\theta_{d+1}} + \beta(\theta)))/(1 + \sum_{i=1}^{d}\lambda_i - \frac{h_t}{2}\delta(x))$$

The above stencil elements are all that we require to prove Theorem 4.1. Recall that $\hat{M}_h^H = \hat{S}_h^{\nu_2}(\hat{I}_h - \hat{I}_H^h\hat{L}_H^{-1}\hat{I}_h^H F_h\hat{L}_h)\hat{S}_h^{\nu_1}$. From the structure of the equation $u_t = \Delta u + \delta(x)u$, we can treat it as a perturbation of the d-dimensional heat equation. We will follow this trend in the representation for $(\hat{M}_h^H)^{\Delta+\delta}$. It can be represented as

$$(\hat{M}_h^H)^{\Delta+\delta} = (\hat{S}_h + \hat{S}_h^{\delta})^{\nu_2}[\hat{I}_h - \hat{I}_H^h(\hat{L}_H^{-1} + \hat{L}_H^{-\delta})\hat{I}_h^H F_h(\hat{L}_h + \hat{L}_h^{\delta})](\hat{S}_h + \hat{S}_h^{\delta})^{\nu_1}.$$

Expanding $(\hat{M}_h^H)^{\Delta+\delta}$, and considering the difference between $\hat{M}_h^H$ and $(\hat{M}_h^H)^{\Delta+\delta}$,

we have

$$(\hat{M}_h^H)^{\Delta+\delta} - \hat{M}_h^H = [(\hat{S}_h + \hat{S}_h)^{\nu_2} - \hat{S}_h^{\nu_2}][\hat{E}_{2G} - F_h(\hat{I}_H^h \hat{L}_H^{-1} \hat{I}_h^H \hat{L}_h^\delta + \hat{I}_H^h \hat{L}_H^{-\delta} \hat{I}_h^H \hat{L}_h$$
$$+ \hat{I}_H^h \hat{L}_H^{-\delta} \hat{I}_h^H \hat{L}_h^\delta)](\hat{S}_h + \hat{S}_h^\delta)^{\nu_1} + \hat{S}_h^{\nu_2} \hat{E}_{2G}[(\hat{S}_h + \hat{S}_h^\delta)^{\nu_1} - \hat{S}_h^{\nu_1}]$$
$$- \hat{S}_h^{\nu_2} F_h(\hat{I}_H^h \hat{L}_H^{-1} \hat{I}_h^H \hat{L}_h^\delta + \hat{I}_H^h \hat{L}_H^{-\delta} \hat{I}_h^H \hat{L}_h$$
$$+ \hat{I}_H^h \hat{L}_H^{-\delta} \hat{I}_h^H \hat{L}_h^\delta)(\hat{S}_h + \hat{S}_h^\delta)^{\nu_1}.$$

Taking the Euclidean norm of both sides and expanding gives us the bound

$$\|(\hat{M}_h^H)^{\Delta+\delta} - \hat{M}_h^H\| \leq (\nu_2 \|\hat{S}_h^\delta\| + O(\|\hat{S}_h^\delta\|^2))(\|\hat{E}_{2G}\| + F_h(\|\hat{L}_H^{-1}\| \|\hat{L}_h^\delta\|$$
$$+ \|\hat{I}_H^h \hat{L}_H^{-\delta} \hat{I}_h^H \hat{L}_h\| + \|\hat{I}_H^h \hat{L}_H^{-\delta} \hat{I}_h^H \hat{L}_h^\delta\|))(1 + \nu_1 \|\hat{S}_h^\delta\|$$
$$+ O(\|\hat{S}_h^\delta\|^2)) + F_h(\|\hat{L}_H^{-1}\| \|\hat{L}_h^\delta\| + \|\hat{I}_H^h \hat{L}_H^{-\delta} \hat{I}_h^H \hat{L}_h\|$$
$$+ \|\hat{I}_H^h \hat{L}_H^{-\delta} \hat{I}_h^H \hat{L}_h^\delta\|)(1 + \nu_1 \|\hat{S}_h^\delta\| + O(\|\hat{S}_h^\delta\|^2))$$
$$+ \|\hat{E}_{2G}\|(\nu_1 \|\hat{S}_h^\delta\| + O(\|\hat{S}_h^\delta\|^2))$$

We need bounds on a number of operators. Making use of the conditions of the theorem, we have $\|\hat{E}_{2G}\| < \Xi$ and $\|\hat{L}_H^{-1}\| < \frac{1}{\epsilon}$. By inspection of (11,15), we immediately see that $\|\hat{L}_h^\delta\| < h_t \delta$. What remains is to obtain bounds on $\|\hat{S}_h^\delta\|$, $\|\hat{I}_H^h \hat{L}_H^{-\delta} \hat{I}_h^H \hat{L}_h\|$, and $\|\hat{I}_H^h \hat{L}_H^{-\delta} \hat{I}_h^H \hat{L}_h^\delta\|$.

We begin with $\|\hat{S}_h^\delta\|$. We note that the smoothing property $\alpha < 1$ implies $\beta < 1$. Using the assumption of $h_t \delta < \Lambda$, we can deduce from results (13,14,17,18) that $_{ie}\alpha_\delta < \frac{h_t \delta}{1+\Lambda}$, $_{ie}\beta_\delta < \frac{3h_t \delta}{1+\Lambda}$, $_{cn}\alpha_\delta < \frac{h_t \delta}{1+\Lambda/2}$, $_{cn}\beta_\delta < \frac{3h_t \delta}{1+\Lambda/2}$, and, therefore, $\|\hat{S}_h^\delta\| < \frac{4h_t \delta}{1+\Lambda/2}$.

Moving on to $\|\hat{I}_H^h \hat{L}_H^{-\delta} \hat{I}_h^H \hat{L}_h\|$, we start by observing that

$$\hat{I}_H^h \hat{L}_H^{-\delta} \hat{I}_h^H \hat{L}_h = F_h^{-1} \hat{I}_H^h \hat{L}_H^{-\delta} \hat{L}_H \hat{I}_h^H [\hat{I}_H^h L_H^{-1} \hat{I}_h^H F_h \hat{L}_h] = F_h^{-1} \hat{I}_H^h \hat{L}_H^{-\delta} \hat{L}_H \hat{I}_h^H [\hat{I}_h - \hat{E}_{2G}].$$

This gives us

$$\|\hat{I}_H^h \hat{L}_H^{-\delta} \hat{I}_h^H \hat{L}_h\| < F_h^{-1}(1+\Xi)\|\hat{I}_H^h \hat{L}_H^{-\delta} \hat{L}_H \hat{I}_h^H\| < F_h^{-1}(1+\Xi)\|\hat{L}_H^{-\delta} \hat{L}_H\|$$
$$< \frac{F_h^{-1}(1+\Xi)h_t \delta}{\epsilon - h_t \delta} < (1+\Xi)\frac{2F_h^{-1}}{\epsilon} h_t \delta.$$

Finding a bound for $\|\hat{I}_H^h \hat{L}_H^{-\delta} \hat{I}_h^H \hat{L}_h^\delta\|$ follows a similar process. We have

$$\hat{I}_H^h \hat{L}_H^{-\delta} \hat{I}_h^H \hat{L}_h^\delta = \hat{I}_H^h \hat{L}_H^{-\delta} \hat{I}_h^H \hat{L}_h^{\Delta+\delta} - \hat{I}_H^h \hat{L}_H^{-\delta} \hat{I}_h^H \hat{L}_h.$$

We have a bound for the second term and using the same technique for the first term, we find its bound is half of that of the second. This gives us $\|\hat{I}_H^h \hat{L}_H^{-\delta} \hat{I}_h^H \hat{L}_h^\delta\| < (1+\Xi)\frac{3F_h^{-1}}{\epsilon} h_t \delta$.

Making use of these bounds, we obtain

$$|\rho[\hat{M}_h^H] - \rho[(\hat{M}_h^H)^{\Delta+\delta}]| \leq (\frac{4\nu_2 h_t \delta}{1 + \Lambda/2} + O(h_t^2 \delta^2))(\Xi + \frac{F_h^{-1}}{\epsilon}(1 + 5(1 + \Xi))h_t \delta$$

$$\times (1 + \frac{4\nu_1 h_t \delta}{1 + \Lambda/2} + O(h_t^2 \delta^2)) + \frac{F_h^{-1}}{\epsilon}(1 + 5(1 + \Xi))h_t \delta$$

$$\times (1 + \frac{4\nu_1 h_t \delta}{1 + \Lambda/2} + O(h_t^2 \delta^2)) + \Xi(\frac{4\nu_1 h_t \delta}{1 + \Lambda/2} + O(h_t^2 \delta^2))$$

Combining all terms of order $O(h_t^2 \delta^2)$ and higher, we have the desired result.

$$|\rho[\hat{M}_h^H] - \rho[(\hat{M}_h^H)^{\Delta+\delta}]| \leq [\frac{4(\nu_1 + \nu_2)}{1 + \Lambda/2}\Xi + \frac{1 + 5(1 + \Xi)}{F_h \epsilon} + O(h_t \delta)]h_t \delta$$

References

[1] Howison, Sam. *Barrier Options* Lecture Notes. Oxford Centre for Industrial and Applied Mathematics. http://people.maths.ox.ac.uk/howison /barriers.pdf

[2] Shreve, Steven. *Stochastic Calculus for Finance II: Continuous-Time Models* Springer Finance. 1st ed. June 2004. ISBN: 978-0387401010

[3] Ugur, Omur. *Introduction to Computational Finance* Imperial College Press; December 2008. ISBN: 978-1848161924

[4] Zvan, R.; Vetzal, K.; Forsyth, P. *PDE methods for pricing barrier options* J. Econ. Dyn. Control 24, 15631590. (2000)

[5] Østerby, Ole. *Five ways of reducing the Crank-Nicolson oscillations.* BIT, 43 (2003), pp. 811-822.

[6] Trottenberg, Ulrich; Oosterlee, Cornelis; Schuller, Anton; *Multigrid* . Academic Press; 1st Ed. 2000 ISBN: 978-0127010700

[7] Horton, G.; Vandewalle, S. *A Space-Time Multigrid Method for Parabolic Partial Differential Equations.* SIAM J. Sci. Comput. Vol. 16, No. 4, pp. 848-864, July 1995

[8] Zhao, Yao. *Fourier Analysis and Local Fourier Analysis for Multigrid Methods* Masters Thesis. Johannes Kepler Universität. July 2009

[9] Brandt, A. *Multi-level adaptive solutions to boundary-value problems* Math. Comp., 31 (138): 333390, 1977.

[10] Van der Vegt, J. J. W.; Rhebergen, S. *hp-Multigrid as Smoother algorithm for higher order discontinuous Galerkin discretizations of advection dominated flows: Part I. Multilevel analysis* Journal of Computational Physics. Volume 231, Issue 22, September 2012

[11] Corradi, V., Distaso, W. *Deterministic versus stochastic volatility* Working Paper. 2007